A Quantum Monte Carlo Study of the Reactions of CH with Acrolein

Srimanta Pakhira,[†,§] Benjamin S. Lengeling,[†,§,⊥] Olayinka Olatunji-Ojo,[‖] Michel Caffarel,[⊥] Michael Frenklach,[#,‡] and William A. Lester, Jr.*[,†,§]

[†]Chemical Sciences Division (CSD), and [‡]Environmental Energy Technologies Division, Lawrence Berkeley National Laboratory, Berkeley, California 94720, United States

[§]Kenneth S. Pitzer Center for Theoretical Chemistry, Department of Chemistry, and [‖]College of Chemistry, University of California, Berkeley, California 94720-1460, United States

[⊥]Laboratoire de Chimie et Physique Quantiques, CNRS-IRSAMC, Université de Toulouse, Toulouse F-31062, France

[#]Department of Mechanical Engineering, University of California, Berkeley, California 94720-1740, United States

ABSTRACT: To assist understanding of combustion processes, we have investigated reactions of methylidyne (CH) with acrolein (CH_2CHCHO) using the quantum Monte Carlo (QMC) and other computational methods. We present a theoretical study of the major reactions reported in a recent experiment on the subject system. Both DFT and MP2 computations are carried out, and the former approach is used to form the independent-particle part of the QMC trial wave function used in the diffusion Monte Carlo (DMC) variant of the QMC method. In agreement with experiment, we find that the dominant product channel leads to formation of C_4H_4O systems + H with leading products of furan + H and 1,3-butadienal + H. Equilibrium geometries, atomization energies, reaction barriers, transition states, and heats of reaction are computed using the DFT, MP2, and DMC approaches and compared to experiment. We find that DMC results are in close agreement with experiment. The kinetics of the subject reactions are determined by solving master equations with the MultiWell software suite.
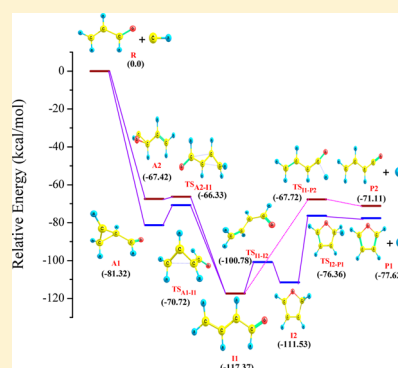
1. INTRODUCTION

Acrolein (CH_2CHCHO) is the simplest β-unsaturated aldehyde present in the atmosphere and is one of the major pollutants produced during biodiesel combustion. It plays an important role in combustion chemistry, including the oxidation of dienes,[1−6] and in atmospheric chemistry. In the latter case, anthropogenic emission of the pollutant butadiene has been found to lead to significant detrimental consequences for human health. Acrolein is also directly connected to biological oxidation processes due to its electrophilicity and reactivity and is a strong irritant for the skin, eyes, and nasal passages.[7] The presence of acrolein in the atmosphere is due to incomplete combustion of petroleum, plastics, and biomass,[8−13] together with increased use of biodiesel and ethanol—gasoline blends.[14] It is important to assess how the increased oxygen content of such fuels affects the absolute and relative concentrations of aldehydes emitted due to the use of biodiesels.[14] The high reactivity of CH leads to its significant role in various fields of science including interstellar chemistry, combustion chemistry, and planetary atmospheres[15−19] with report of detection in the interstellar medium,[20−22] comets,[23] stellar atmospheres,[24,25] and flames.[26]

Recently, Lockyear et al.[27] measured product formation in the CH + acrolein reaction using tunable vacuum-ultraviolet (VUV) synchrotron radiation and multiplexed photoionization mass spectrometry. They computed the structures, vibrational modes, and transition intensities of the molecules of interest at the B3LYP[28−31]/6-311++G(2d,p) level of theory and the CBS-QBS[32,33] composite method. Rate coefficients and branching fractions were computed using RRKM[34−37] theory. Previously, Leone and collaborators carried out a series of product detection studies of reactions of CH with small, unsaturated hydrocarbons[38,39] (acetylene (C_2H_2), ethylene (C_2H_4), allene (C_3H_4), propyne (C_3H_4), and propene (C_3H_6)), carbonyl-containing species acetaldehyde[40] and acetone,[41] as well as the cyclic nitrogen-containing pyrrole.[42]

Accurately modeling these systems requires precise chemical data in the form of reaction rate coefficients and product branching fractions. The goal of the present effort is to assess the validity of previous theoretical findings with more extensive computations using alternative methods. We are particularly interested in ascertaining whether the quantum Monte Carlo (QMC) method can add to understanding of the reaction mechanisms for this system.[43−46]

The QMC method is a stochastic approach for solving the Schrodinger equation.[47,48] It has been shown to produce highly accurate total energies of the ground state of many-electron systems in the diffusion MC (DMC) variant of the method. The DMC approach has been shown to scale better with system size than other ab initio methods of comparable
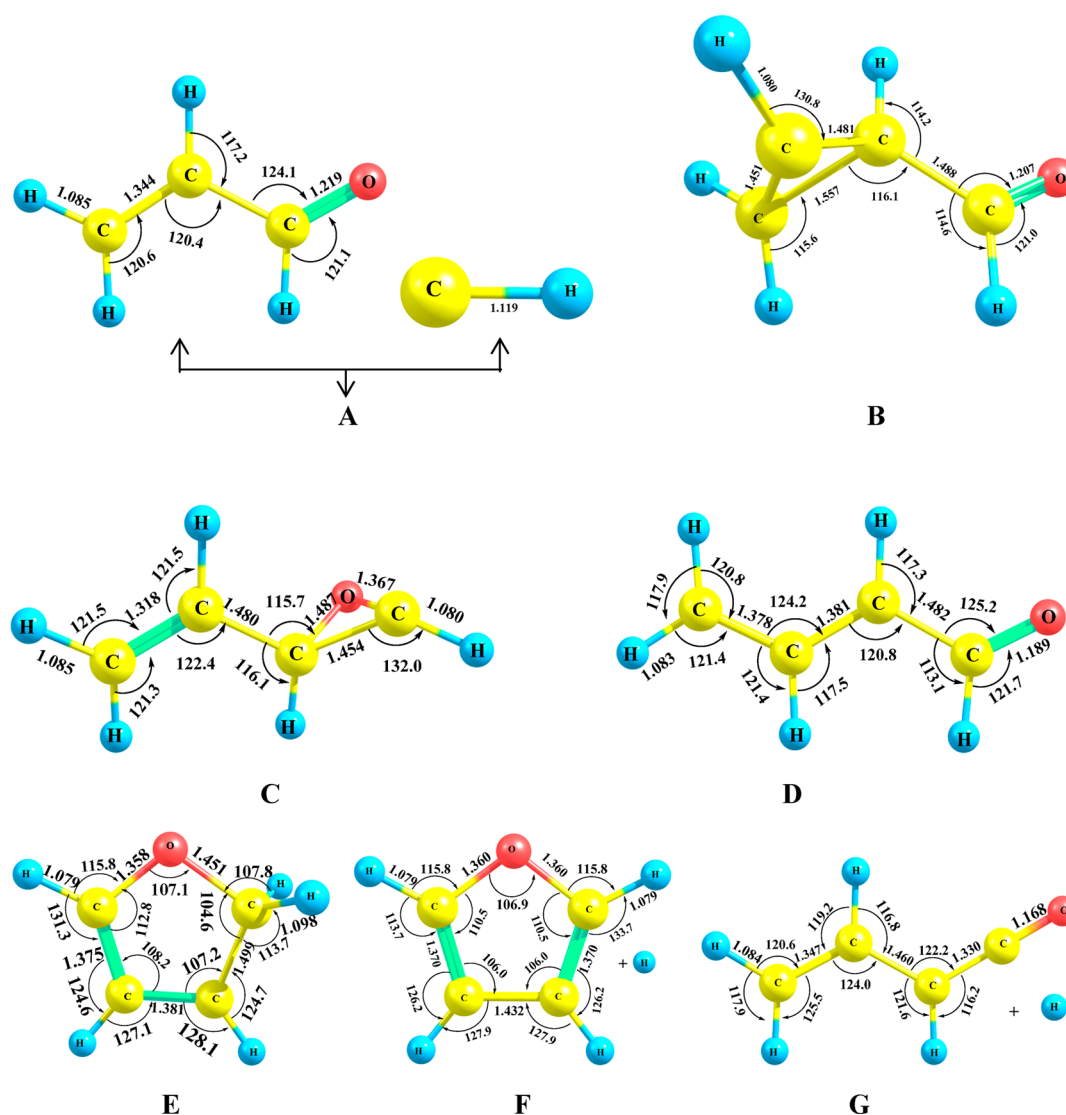
Figure 1. Optimized geometries with geometrical parameters calculated at MP2/6-311++G(d,p) level of theory for the species (first row, (A) reactants **R**, (B) first adduct **A1**; second row, (C) second adduct **A2**, (D) first intermediate **I1**; third row, (E) second intermediate **I2**, (F) first product **P1**, (G) second product **P2**) involved in the subject reaction.

accuracy, in particular, CCSD(T). In the approach, the trial wave function, which governs the accuracy of the method, is typically chosen as a product of a determinantal expansion and a correlation function, the latter containing explicit interparticle distances.

Here, the structures, transition states, reaction pathways, relative energies, atomization energies, heats of reaction, and heats of formation are computed using the DMC, B3LYP,[28−31] M06-2X,[49] and MP2[50] methods. We consider the reaction paths that lead to the two main product channels as reported by Lockyear et al.[27] The dominant product channel is the formation of C_4H_4O systems + H with leading products of furan + H and 1,3-butadienal + H. We have used the aforementioned methods to compute critical points and stable intermediates of the reaction pathways. In addition, we have calculated heats of reaction and atomization energies of the stable molecular systems.

2. COMPUTATIONAL DETAILS

2.1. Electronic Structure Calculations. The geometries of reactants and products, and relevant stationary points,

including local minima and first-order saddle points, were obtained with the B3LYP,[28−31] M06-2X,[49] and MP2[50] methods with the 6-311++G(d,p)[51] basis set. Harmonic vibrational frequencies at the optimized geometries and saddle points were analyzed at the respective levels of theory to reveal the nature of the stationary points. Intrinsic reaction coordinate (IRC) calculations[52,53] were carried out to confirm transition state structures. The DFT method was used for geometry optimization because densities and energies obtained with the method are less affected by spin contamination than other approaches.[54−60] These calculations were performed with the general purpose electronic structure quantum chemistry program GAMESS.[61,62]

2.2. QMC Computations and Trial Wave Functions. The DMC calculations were carried out with the Zori[63] code. The B3LYP method was used to construct the independent-particle part of the DMC trial wave functions, and these in turn were multiplied by a 15-parameter Schmidt−Moskowitz−Boys−Handy[64,65] (SMBH) correlation function. The SMBH function contains two- and three-body terms involving explicit electron−electron, electron−nucleus, and electron−other−
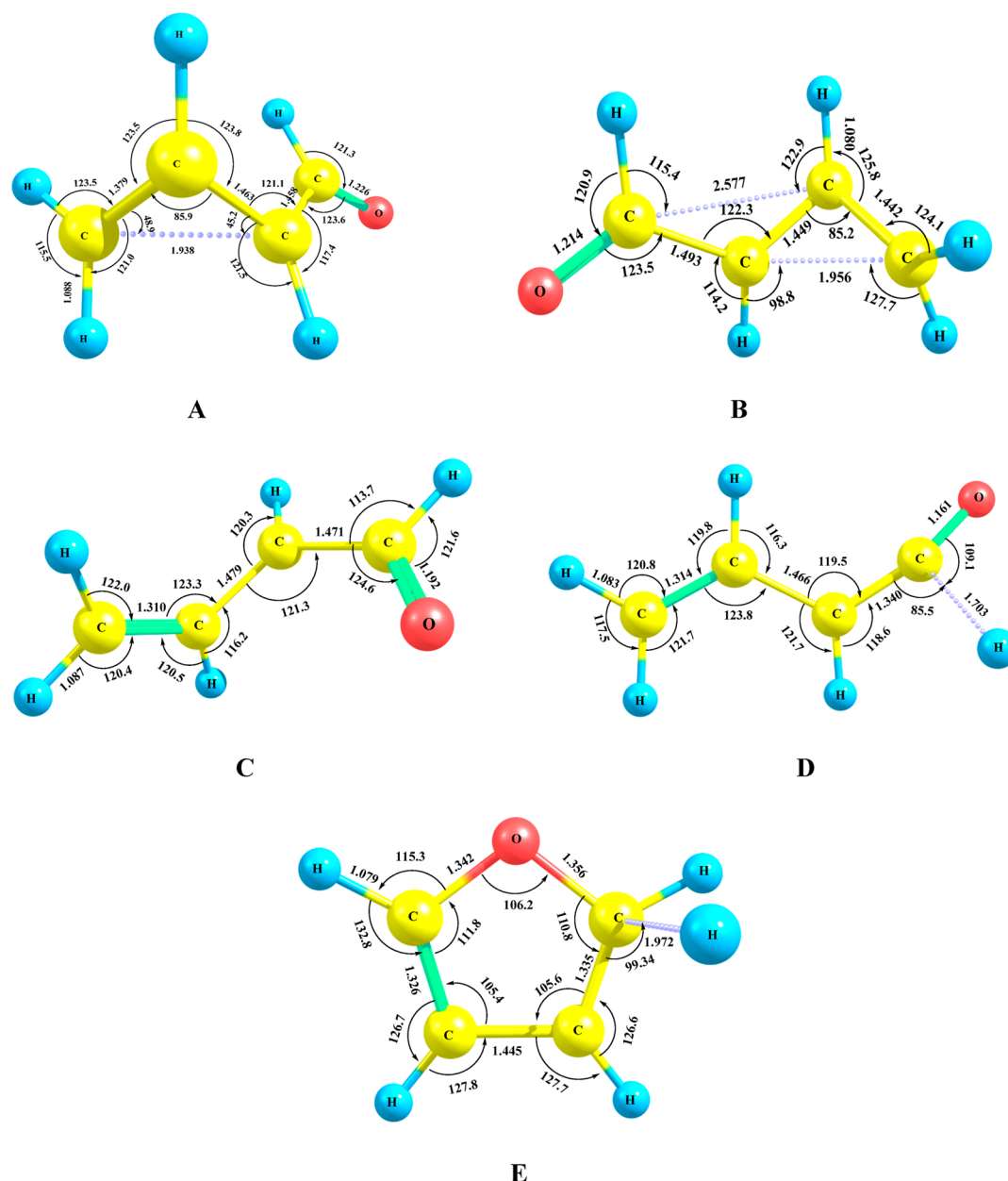
Figure 2. Optimized geometries with geometrical parameters calculated at MP2/6-311++G(d,p) level of theory for all of the transition states (TS) (first row, (A) transition state TS_{A1-I1}, (B) transition state TS_{A2-I1}; second row, (C) transition state TS_{I1-I2}, (D) transition state TS_{I1-P2}; third row, (E) transition state TS_{I2-P1}) involved in the subject reaction.

nucleus distances and serves to reduce the variance in the local energy and to improve stability of the computations. The DMC calculations were performed at three time steps: 0.004, 0.002, and 0.001 hartree^{-1}. For each run, a population of 24 000 walkers was used. Extrapolation[66] to zero time step was carried out to minimize time step bias, which, given the nature of the Umrigar et al. algorithm,[67] is small at the time steps chosen. Weighted quadratic least-squares fits were used for the extrapolation.

2.3. Thermochemistry. Heats of formation at 0 K ($\Delta_f H_0^o$) and 298 K ($\Delta_f H_{298}^o$) for the systems involved in the subject reaction were calculated following Nicoleides et al.[68] with the B3LYP, M06-2X, MP2, and DMC methods. For this purpose, we used literature values of $\Delta_f H_0^o$ for H (51.63 kcal/mol), C (169.98 kcal/mol), and O (58.99 kcal/mol).[69,70] The atomization energies, heats of formation, and heats of reaction at 0

and 298 K were computed in the usual way; see, for example, Kollias et al.[71]

2.4. MultiWell Simulation. Reaction rate coefficients of the CH/acrolein reaction system were computed using the latest release (v.2014.1) of the MultiWell software suite.[72−74] MultiWell solves the one-dimensional time-dependent energy-transfer master equations for a multiwell or multichannel unimolecular reaction system using a Monte Carlo stochastic method.[75,76] MultiWell simulations yield time-dependent concentrations, vibrational distributions, and rate constants as functions of temperature and pressure for unimolecular reaction systems that consist of multiple stable species, multiple reaction channels that interconnect, and multiple dissociation channels from each stable species. Centrifugal force corrections can be added and tunneling effects can be included to simulate slow intramolecular vibrational energy redistribution. In

Table 1. Relative Energies of Molecular Systems Arising in the Subject Reactions Computed by Selected Methods (kcal/mol)

|	methods				
species	B3LYP	M06-2X	MP2	DMC	others[a]
$CH+CH_2CHCHO$ (**R**)	0	0	0	0	0
C=C cyclo-adduct (**A1**)	−80.16	−89.06	−86.49	−81.32 ± 0.94	−82.89
C=O cyclo-adduct (**A2**)	−66.47	−73.53	−67.21	−67.42 ± 0.97	−70.48
TS$_{A1-I1}$	−67.31	−84.67	−64.84	−70.72 ± 0.84	−69.22
TS$_{A2-I1}$	−61.96	−66.18	−58.39	−66.33 ± 1.02	−60.59
but-3-enal-2-yl (**I1**)	−116.71	−117.88	−105.12	−117.37 ± 0.81	−117.14
furan-H adduct (**I2**)	−108.08	−114.63	−104.42	−111.53 ± 1.10	−113.17
TS$_{I1-I2}$	−103.48	−105.88	−98.32	−100.78 ± 0.89	−91.09
TS$_{I1-P2}$	−65.87	−66.20	−60.19	−67.72 ± 0.88	−63.96
TS$_{I2-P1}$	−75.16	−82.64	−74.43	−76.36 ± 1.08	−79.61
furan + H (**P1**)	−74.64	−84.64	−89.98	−77.62 ± 0.83	−81.88
1,3-butadienal + H (**P2**)	−66.74	−70.99	−76.20	−71.11 ± 0.78	−67.71

[a]Reference 27.
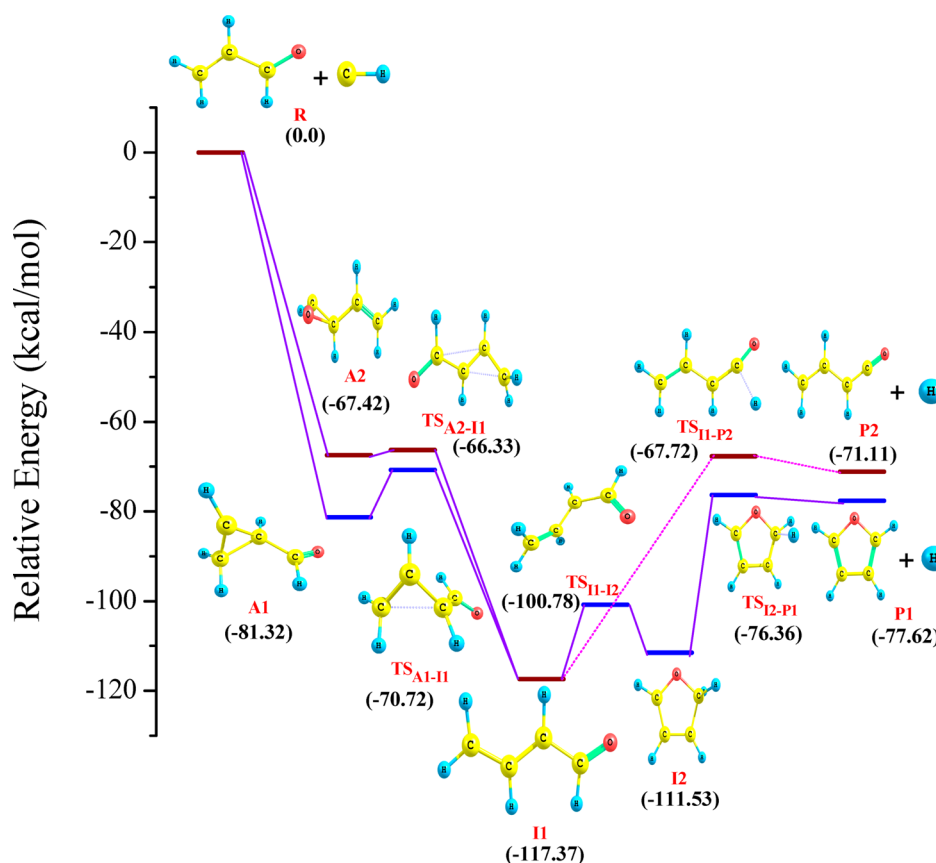
Figure 3. Reaction pathways calculated at DMC level of theory for the subject reaction.

addition, Densum of the MultiWell's software suite[72−74] provides sums and densities of states via the Stein−Rabinovitch extension of the Beyer−Swinehart algorithm. In the MultiWell simulation, harmonic and anharmonic vibrations and classical and quantized free rotations are taken into account.

3. RESULTS AND DISCUSSION

Optimized geometries of the molecules and transition states involved in the subject reaction were determined using the B3LYP, M06-2X, and MP2 methods with the 6-311++G(d,p) basis set. The MP2/6-311++G(d,p) optimized structures and associated geometrical parameters are shown in Figure 1A−G,

and the transition states computed with the same approach are depicted in Figure 2A−E.

Table 1 presents the relative energies of all minima, intermediates, transition states, and products involved in the subject reaction obtained with the B3LYP, M06-2X, MP2, and DMC methods and includes the findings of Lockyear et al.[27] Note that the values associated with these systems are relative to the total energy of reactants CH + CH₂CHCHO, here designated **R**, at each level of theory. The DMC reaction pathways are depicted in Figure 3, and the Lockyear et al. reaction pathways are shown in Figure 4. We have considered the two entrance pathways that form the cyclo-adducts (**A1** and **A2**). In cyclo-addition to an unsaturated hydrocarbon bond, it
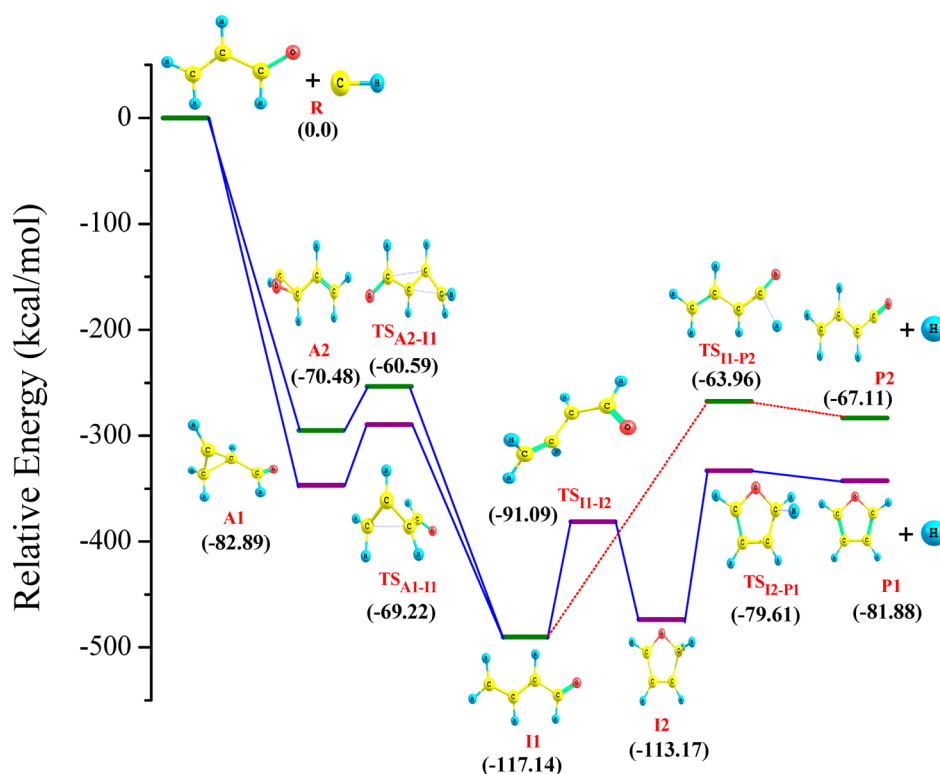
Figure 4. Lockyear et al.[27] reaction pathways calculated at CBS-QB3 level of theory for the subject reaction.

Table 2. Atomization Energies of Molecular Systems Arising in the Subject Reactions Computed by Selected Methods (kcal/mol)

	methods				others	
species	B3LYP	M06-2X	MP2	DMC	expt.	theor.
CH radical	79.82	78.67	79.71	79.54 ± 0.11	79.9[a]	80,[b,c,d] 83.3−83.8[e]
CH_2CHCHO	788.40	787.85	789.91	789.31 ± 0.34		
C=C cyclo-adduct	942.98	949.28	946.65	942.94 ± 0.42		
C=O cyclo-adduct	929.13	933.48	927.59	933.42 ± 0.53		
but-3-enal-2-yl	978.72	977.84	972.35	976.78 ± 0.23		
furan-H adduct	968.98	973.52	970.21	971.22 ± 0.52		
furan	948.73	949.28	948.90	950.46 ± 0.38	950.6 ± 0.2[f]	915.5−1012.5,[g] 950.0 ± 0.5[g]
1,3-butadienal	930.17	930.79	937.09	929.60 ± 0.37		

[a]Reference 77. [b]Reference 78. [c]Reference 79. [d]Reference 80. [e]Reference 81. [f]Reference 82. [g]Reference 87.

is well accepted that the cyclo-addition is followed by ring opening and the cyclic intermediate is extremely short-lived.[38,39] Acrolein with both C=O and C=C bonds presents an interesting case because of the competition between cyclo-addition of CH at the C=O and C=C bonds.

The highly reactive CH interacts with acrolein in two ways. In one case, CH breaks a C=C bond and forms a C=C cyclo-adduct (**A1**). In the other case, CH breaks the C=O bond and forms the C=O cyclo-adduct (**A2**). The relative energy of the two cyclo-adducts computed by DMC is in reasonable accord with Lockyear et al.[27] Formation of the cyclo-adducts proceeds through but-3-enal-2-yl (**I1**, C_4H_5O) as an intermediate. The DMC relative energies of the transition structures **TS$_{A1−I1}$** and **TS$_{A2−I1}$** that connect **A1** and **A2** with but-3-enal-2-yl (**I1**) are in reasonable accord with Lockyear et al.[27] The molecule but-3-enal-2-yl (**I1**) reacts in two ways and produces two H elimination channels. In one case, but-3-enal-2-yl (**I1**) produces the furan-H adduct (**I2**, C_4H_5O), which is followed by H elimination yielding furan (C_4H_4O) as the product. In this case,

we found two transition states (TS), **TS$_{I1−I2}$** and **TS$_{I2−P1}$**, which connect but-3-enal-2-yl (**I1**) and the furan-H adduct (**I2**), and the furan-H adduct (**I2**) and furan + H (**P1**), respectively. In the other case, **I1** eliminates H directly leading to **TS$_{I1−P2}$** and forms 1,3-butadienal + H (**P2**) as product. The DMC relative energies for all transition states, products, and intermediates are also in accord with Lockyear et al.[27] These two reaction pathways are the main competing paths found experimentally by Lockyear et al. The latter also calculated specific rate coefficients for these products, **P1** and **P2**, by RRKM theory.[34−37] The DMC and other-method results show that the dominant products formed in this reaction are furan + H (**P1**) and 1,3-butadienal + H (**P2**).

The atomization energy (E_a) of the stable species involved in this reaction has been computed with the aforementioned methods. These values are listed in Table 2 along with earlier experimental and theoretical results. For CH, the DMC E_a and values from other methods lie within 0.4 kcal/mol of Huber

Table 3. Heats of Formation ($\Delta_f H_0^o$) at 0 K of Molecular Systems Arising in the Subject Reactions Computed by Selected Methods (kcal/mol)

species	methods				others	
	B3LYP	M06-2X	MP2	DMC	expt.	theor.
CH radical	141.77	142.94	141.90	142.06 ± 0.12	141.6 ± 14,[a] 141.7[b]	141.1[b]
CH$_2$CHCHO	−12.95	−12.40	−14.46	−13.86 ± 0.37		−14.25,[c] −13.9 ± 2.42[d]
C=C cyclo-adduct	54.08	47.78	50.31	54.12 ± 0.58		
C=O cyclo-adduct	67.93	63.58	69.47	63.64 ± 0.63		
but-3-enal-2-yl	18.34	19.22	24.71	20.28 ± 0.36		
furan-H adduct	28.08	23.54	26.85	25.84 ± 0.37		
furan	−3.30	−3.85	−3.47	−5.03 ± 0.40	−5.2 ± 0.2[a]	−4.6 ± 0.5[e]
1,3-butadienal	15.26	14.64	8.34	15.83 ± 0.39		

[a]Reference 82. [b]Reference 83. [c]Reference 84. [d]Reference 85. [e]Reference 87.

Table 4. Heats of Formation ($\Delta_f H_{298}^o$) at 298 K of Molecular Systems Arising in the Subject Reactions Computed by Selected Methods (kcal/mol)

species	methods				others	
	B3LYP	M06-2X	MP2	DMC	expt.	theor.
CH radical	142.57	143.72	142.68	142.85 ± 0.12	142.5 ± 0.3[a]	141.9,[b] 142.4–143.1[c]
CH$_2$CHCHO	−15.43	−14.88	−16.94	−16.34 ± 0.37		−15.6,[d] −16.70 ± 1.0,[d] −16.5 ± 2.4[e]
C=C cyclo-adduct	50.66	44.37	48.89	50.70 ± 0.58		
C=O cyclo-adduct	64.53	60.18	66.07	60.24 ± 0.63		
but-3-enal-2-yl	15.08	15.96	21.54	17.02 ± 0.36		
furan-H adduct	24.21	19.67	26.85	21.96 ± 0.37		
furan	−6.55	−7.1	−6.72	−8.28 ± 0.40	−8.3 ± 0.2[f]	−7.7 ± 0.5[c]
1,3-butadienal	13.00	12.38	6.08	13.57 ± 0.39		

[a]Reference 83. [b]Reference 88. [c]Reference 86. [d]Reference 84. [e]Reference 85. [f]Reference 82.

Table 5. Heats of Reaction (ΔH_{rxn}^o) Formed in the Subject Reaction Computed by Selected Methods (kcal/mol)

species	methods			
	B3LYP	M06-2X	MP2	DMC
furan + H (**P1**)	−82.06	−84.31	−80.23	−83.16 ± 0.56
1,3-butadienal + H (**P2**)	−62.51	−64.83	−68.03	−61.31 ± 0.55

and Herzberg.[77] The latter include computations of Pople et al.,[78] Curtiss et al.,[79] Grossman,[80] and Feller and Peterson.[81]

The DMC E_a of acrolein as well as both cyclo-adducts (**A1** and **A2**), but-3-enal-2-yl (**I1**), furan-H adduct (**I2**), furan, and 1,3-butadienal are also consistent with the B3LYP and MP2 results; see Table 2. The furan E_a values from B3LYP and MP2 are close to each other but differ notably from the M06-2X and DMC values that are in turn close to each other. The DMC E_a is in excellent agreement with experiment.[82] The DMC E_a for 1,3-butadienal and the DFT results are in good agreement; the MP2 result is notably higher.

Heats of formation at 0 K ($\Delta_f H_0^o$) for the systems being discussed are reported in Table 3, and heats of formation at 298 K ($\Delta_f H_{298}^o$) are given in Table 4. The CH $\Delta_f H_0^o$ from DMC and other approaches reproduce the experiments of Pedley[82] at both 0 and 298 K, and for Ruscic et al.[83] No experimental value of $\Delta_f H_0^o$ for acrolein is available. The DMC calculated $\Delta_f H_0^o$ of acrolein is close to the values of Asatryan et al.[84] and of Li and Baer,[85] while the MP2 result agrees well with the previously computed values of Rodriquez et al.[86] There are no experimental or theoretical values of heats of formation for the cyclo-adducts. Computed values for these systems are contained in the respective tables.

The heats of reaction (ΔH_{rxn}^o) of both of the products formed in the subject reactions are given in Table 5. It is clear from the table that the reaction between the CH and acrolein

molecule is exothermic. There are no experimental or theoretical results for comparison. The DFT (B3LYP and M06-2X) ΔH_{rxn}^o values are in good agreement with the DMC value. The ΔH_{rxn}^o of the first product, furan + H (**P1**), calculated at the MP2 level of theory is about 3 kcal/mol lower than the DMC result. The ΔH_{rxn}^o of the second product 1,3-butadienal + H (**P2**) calculated at the MP2 level is about 6.72 kcal/mol lower than the DMC calculated value. The ΔH_{rxn}^o calculated at the DMC level of theory of furan + H (**P1**) is about 22 kcal/mol lower than the 1,3-butadienal + H (**P2**) product.

The predicted branching fractions of two products (**P1** and **P2**) formed in this reaction were determined from the ratios of species fractions computed with the MultiWell code.[72−74] The species fractions were level at a time scale of 10^{-5} s. The key inputs to the MultiWell simulations are reaction barriers, frequencies, and moments of inertia. The parameters for each simulation are chosen to emulate the conditions of the experiments performed by Lockyear et al.[27] The pressure is set to 4 Torr at a temperature of 298 K, using a He collider with empirical Lennard-Jones parameters. Approximately 1000 simulations were carried out following Gillespie's stochastic simulation algorithm.[75,76] An energy grain of 5 cm^{-1} was utilized in each simulation. Energy grain size, simulation time, and the Lennard-Jones parameters for wells and colliders were varied to check the sensitivity of the simulation to these
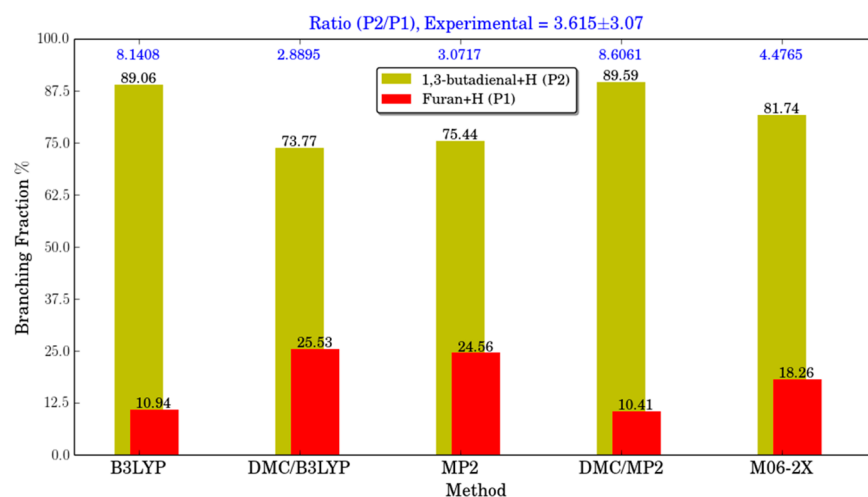
Figure 5. Computed branching fractions for products of the main reaction channels are compared at various levels of theory. At the top of the figure, the product branching ratio is given for each of the theoretical methods. This is the preferred quantity to compare with experiment. It is shown that the product branching ratios computed at the DMC level with B3LYP frequencies (DMC/B3LYP), MP2, and M06-2X levels of theory all lie within experimental error. The remaining methods, B3LYP and DMC with MP2 frequencies (DMC/MP2), lie outside of experimental uncertainty.

parameters; product branching fractions deviated at most by 0.5%, giving confidence that the parameters are chosen correctly. The collisional energy transfer is described by the exponential-down model with $\langle \Delta E_{down} \rangle$ = 250 cm^{-1}. The quantity $\langle \Delta E_{down} \rangle$ was varied across a wide range of values, 100−1000, to test if its value affected the results. The test showed rather small deviations, about 0.025 in the product fractions.

The simulations are initiated by assuming a barrierless reaction starting from the reactant (**R**) to the adducts (**A1**, **A2**) initiated by a nascent chemical activation energy distribution. For these two forward reactions, no centrifugal force is assumed. For all other forward reactions, a quasi-diatomic centrifugal correction with two adiabatic external rotations was utilized as suggested by the MultiWell algorithm. Quantum rotors are used when the rotational constants are higher than 1 cm^{-1}, and the classical rotor approximation when constants are below this value.

For the DMC simulations, scaled MP2 frequencies and rotational constants were utilized. A summary of results from the MultiWell chemical-activation runs and the branching fraction ratios are shown in Figure 5. For all simulations, the second product (**P2**) dominates the product branching fractions; all lie within the range 75−91% of product formation. Because the branching reported by Lockyear et al.[27] is for the overall reaction pathway, it is not directly comparable to the present findings that address only the two main reactions. Nevertheless, product ratios can provide a qualitative measure of the fit. With this assumption, the experimental product ratio lies in the range of (0.545, 6.685), and hence within a range of acceptable values. Because of the large **P2** product fraction, small deviations in the branching fraction of the first product **P1** can significantly alter the product ratio. Nevertheless, most simulations lie within the experimental range of values. The branching ratios computed with the MP2 method and the DMC method (DMC/B3LYP) using the B3LYP optimized geometry are in good agreement with Lockyear et al.[27] The B3LYP method gives, however, branching ratios that lie outside the experimental range. This is due to poor estimates of molecular frequencies from B3LYP.

A final remark concerns the accuracy of the DMC approach. As is well known,[43] the fundamental error present in DMC is the fixed-node error resulting from the approximate nodes of the trial wave function. Other errors including those arising from the time step choice or the use of a finite population may also be present, but are readily estimated and removed using extrapolation techniques.

In this study, B3LYP nodes of single determinant trial functions were used, and DMC results in close agreement with experiment were found. It is likely, however, that DMC results could be further improved by employing nodes of multi-determinant trial wave functions. However, in view of the great sensitivity observed for the DMC P2/P1 ratio on the optimized geometry used (either B3LYP or MP2, see Figure 5), such a study would require recomputing each reaction path at the multideterminant level. Such a major study is left for future work.

4. CONCLUSIONS

Motivated by the recent VUV synchrotron light and multiplexed photoionization mass spectrometry experiment, we have explored computationally the reaction between CH and acrolein. Reaction pathways, relative energies, atomization energies, heats of formation, and heats of reaction were computed using the B3LYP, M06-2X, MP2, and DMC methods. The DMC atomization energy, heats of formation at 0 and 298 K of the CH and of furan are found to be in excellent agreement with experiment. The main products, furan + H (**P1**) and 1,3-butadienal + H (**P2**), found in the present study agree with the experiments of Lockyear et al. The present study firmly establishes that the hydrogen-loss (C_4H_4O + H) pathway with leading products of furan + H (**P1**) and 1,3-butadienal + H (**P2**) pathway is the main product channel formed.

A MultiWell simulation and branching ratio analysis have also clarified the dominance of product **P2** over product **P1**. The present findings are in accord with the experiment of Lockyear et al. It is confirmed that the predicted H-loss pathway is the major product channel of the reaction to produce the main products **P1** and **P2**.

AUTHOR INFORMATION

Corresponding Author

*Phone: (510) 643-9590. E-mail: walester@berkeley.edu.

Notes

The authors declare no competing financial interest.

ACKNOWLEDGMENTS

REFERENCES

(1) Grosjean, D. Atmospheric Chemistry of Toxic Contaminants. 3. Unsaturated Aliphatics: Acrolein, Acrylonitrile, Maleic Anhydride. *J. Air Waste Manage. Assoc.* **1990**, *40*, 1664−1668.

(2) Berndt, T.; Böge, O. Atmospheric Reaction of OH Radicals with 1,3-Butadiene and 4-Hydroxy-2-butenal. *J. Phys. Chem. A* **2007**, *111*, 12099−12105.

(3) Liu, X.; Jefries, H. E.; Sexton, K. G. Hydroxyl Radical and Ozone Initiated Photochemical Reactions of 1,3-Butadiene. *Atmos. Environ.* **1999**, *33*, 3005−3022.

(4) Tuazon, E. C.; Alvarado, A.; Aschmann, S. M.; Atkinson, R.; Arey, J. Products of the Gas-Phase Reactions of 1,3-Butadiene with OH and NO_3 Radicals. *Environ. Sci. Technol.* **1999**, *33*, 3586−3595.

(5) Tanimoto, H.; Akimoto, H. A New Peroxycarboxylic Nitric Anhydride Identified in the Atmosphere: $CH_2=CHC(O)OONO_2$ (APAN). *Geophys. Res. Lett.* **2001**, *28*, 2831−2834.

(6) Roberts, J. M.; Flocke, F.; Weinheimer, A.; Tanimoto, H.; Jobson, B. T.; Riemer, D.; Apel, E.; Atlas, E.; Donnelly, S.; Stroud, V.; Johnston, K.; Weaver, R.; Fehsenfeld, F. C. Observations of APAN during TexAQS 2000. *Geophys. Res. Lett.* **2001**, *28*, 4195−4198.

(7) Arntz, D.; Fischer, A.; Höpp, M.; Jacobi, S.; Sauer, J.; Ohara, T.; Sato, T.; Shimizu, N.; Schwind, H. Acrolein and Methacrolein. *Ullmann's Encyclopedia of Industrial Chemistry*; Wiley-VCH: Weinheim, 2012.

(8) Bein, K.; Leikauf, G. D. Acrolein - A Pulmonary Hazard. *Mol. Nutr. Food Res.* **2011**, *55*, 1342−1360.

(9) Song, C. L.; Zhao, Z. A.; Lv, G.; Song, J. N.; Liu, L. D.; Zhao, R. F. Carbonyl Compound Emissions from a Heavy-duty Diesel Engine Fueled with Diesel Fuel and Ethanol−diesel Blend. *Chemosphere* **2010**, *79*, 1033−1039.

(10) Esterbauer, H.; Schaur, R. J.; Zollner, H. Chemistry and Biochemistry of 4-Hydroxynonenal, Malonaldehyde and Related Aldehydes. *Free Radical Biol. Med.* **1991**, *11*, 81−128.

(11) Stevens, J. F.; Maier, C. S. Acrolein: Sources, Metabolism, and Biomolecular Interactions Relevant to Human Health and Disease. *Mol. Nutr. Food Res.* **2008**, *52*, 7−25.

(12) Spada, N.; Fujii, E.; Cahill, T. M. Diurnal Cycles of Acrolein and Other Small Aldehydes in Regions Impacted by Vehicle Emissions. *Environ. Sci. Technol.* **2008**, *42*, 7084−7090.

(13) Woodruff, T. J.; Caldwell, J.; Cogliano, V. J.; Axelrad, D. A. Estimating Cancer Risk from Outdoor Concentrations of Hazardous Air Pollutants in 1990. *Environ. Res.* **2000**, *82*, 194−206.

(14) Kohse-Hoinghaus, K.; Osswald, P.; Cool, T. A.; Kasper, T.; Hansen, N.; Qi, F.; Westbrook, C. K.; Westmoreland, P. R. Biofuel Combustion Chemistry: From Ethanol to Biodiesel. *Angew. Chem., Int. Ed.* **2010**, *49*, 3572−3597.

(15) Amin, M. Y.; EI-Nawawy, M. S. The Chemical Evaluation in a Model of Contracting Cloud. *Earth, Moon, Planets* **1996**, *75*, 25−39.

(16) Brownsword, R. A.; Sims, I. R.; Smith, I. W. M.; Stewart, D. W. A.; Canosa, A.; Rowe, B. R. The Radiative Association of CH with H_2: A Mechanism for Formation of CH_3 in Interstellar Clouds. *Astrophys. J.* **1997**, *485*, 195−202.

(17) Miller, J. A.; Bowman, C. T. Mechanism and Modeling of Nitrogen Chemistry in Combustion. *Prog. Energy Combust. Sci.* **1989**, *15*, 287−338.

(18) Miller, J. A.; Kee, R. J.; Westbrook, C. Chemical Kinetics and Combustion Modeling. *Annu. Rev. Phys. Chem.* **1990**, *41*, 345−387.

(19) Canosa, A.; Sims, I. R.; Travers, D.; Smith, I. W. M.; Rowe, B. R. Reactions of the Methylidine Radical with CH_4, $C_2 H_2$, C_2H_4, C_2H_6 and But-1-ene Studied Between 23 and 295 K with a CRESU Apparatus. *Astron. Astrophys.* **1997**, *323*, 644−651.

(20) Turner, B. E.; Zuckerman, B. Microwave Detection of Interstellar CH. *Astrophys. J.* **1974**, *187*, L59−62.

(21) Rydbeck, O. E. H.; Ellder, J.; Irvine, W. M. Radio Detection of Interstellar CH. *Nature* **1973**, *246*, 466−468.

(22) Lien, D. J. A Reanalysis of the Interstellar CH Abundance. *Astrophys. J.* **1984**, *284*, 578−588.

(23) Arpigny, C. Spectra of Comets and Their Interpretation. *Annu. Rev. Astron. Astrophys.* **1965**, *3*, 351−376.

(24) Ridgway, S. T.; Carbon, D. F.; Hall, D. N. B.; Jewell, J. An Atlas of Late-type Stellar Spectra, 2400−2778 Inverse Centimeters. *Astrophys. J. Suppl.* **1984**, *54*, 177−209.

(25) Lambert, D. L.; Gustafsson, B.; Eriksson, K.; Hinkle, K. H. The Chemical Composition of Carbon Stars: I. Carbon, Nitrogen, and Oxygen in 30 Cool Carbon Stars in the Galactic Disk. *Astrophys. J. Suppl.* **1986**, *62*, 373−425.

(26) Thoman, J. W.; McIlroy, A. Absolute CH Radical Concentrations in Rich Low-pressure Methane-oxygen-argon Flames via Cavity Ringdown Spectroscopy of the A(2) Delta-(XII)-I-2 Transition. *J. Phys. Chem. A* **2000**, *104*, 4953−4961.

(27) Lockyear, J. F.; Welz, O.; Savee, D. J.; Goulay, F.; Trevitt, J. A.; Taatjes, A. C.; Osborn, D. L.; Leone, S. R. Isomer Specific Product Detection in the Reaction of CH with Acrolein. *J. Phys. Chem. A* **2013**, *117*, 11013−11026.

(28) Becke, A. D. Density-functional Thermochemistry. III. The Role of Exact Exchange. *J. Chem. Phys.* **1993**, *98*, 5648−5652.

(29) Lee, C.; Yang, W.; Parr, R. G. Development of the Colle-Salvetti Correlation-energy Formula into a Functional of the Electron Density. *Phys. Rev. B* **1988**, *37*, 785−789.

(30) Vosko, S. H.; Wilk, L.; Nusair, M. Accurate Spin-dependent Electron Liquid Correlation Energies for Local Spin Density Calculations: A Critical Analysis. *Can. J. Phys.* **1980**, *58*, 1200−1211.

(31) Stephens, P. J.; Devlin, F. J.; Chabalowski, C. F.; Frisch, M. J. Ab-initio Calculation of Vibrational Absorption and Circular Dichroism Spectra Using Density Functional Force Fields. *J. Phys. Chem.* **1994**, *98*, 11623−11627.

(32) Montgomery, J. A.; Frisch, M. J.; Ochterski, J. W.; Petersson, G. A. A Complete Basis Set Model Chemistry. VI. Use of Density Functional Geometries and Frequencies. *J. Chem. Phys.* **1999**, *110*, 2822−2827.

(33) Montgomery, J. A.; Frisch, M. J.; Ochterski, J. W.; Petersson, G. A. A Complete Basis Set Model Chemistry. VII. Use of the Minimum Population Localization Method. *J. Chem. Phys.* **2000**, *112*, 6532−6542.

(34) Klippenstein, S. J. Variational Optimizations in the Rice-Ramsberger-Kassel-Marcus Theory Calculations for Unimolecular Dissociations with no Reverse Barrier. *J. Chem. Phys.* **1992**, *96*, 367−371.

(35) Klippenstein, S. J.; Marcus, R. A. High Pressure Rate Constants for Unimolecular Dissociation/Free Radical Recombination: Determination of the Quantum Correction via Quantum Monte Carlo Path Integration. *J. Chem. Phys.* **1987**, *87*, 3410−3417.

(36) Wardlaw, D. M.; Marcus, R. A. RRKM Reaction Rate Theory for Transition States of any Looseness. *Chem. Phys. Lett.* **1984**, *110*, 230−234.

(37) Wardlaw, D. M.; Marcus, R. A. Unimolecular Reaction Rate Theory for Transition States of Partial Looseness. II. Implementation and Analysis with Applications to NO_2 and C_2H_6 Dissociations. *J. Chem. Phys.* **1985**, *83*, 3462−3480.

(38) Goulay, F.; Trevitt, A. J.; Meloni, G.; Selby, T. M.; Osborn, D. L.; Taatjes, C. A.; Vereecken, L.; Leone, S. R. Cyclic Versus Linear Isomers Produced by Reaction of the Methylidyne Radical (CH) with Small Unsaturated Hydrocarbons. *J. Am. Chem. Soc.* **2009**, *131*, 993−1005.

(39) Trevitt, A. J.; Prendergast, M. B.; Goulay, F.; Savee, J. D.; Osborn, D. L.; Taatjes, C. A.; Leone, S. R. Product Branching Fractions of the CH + Propene Reaction from Synchrotron Photoionization Mass Spectrometry. *J. Phys. Chem. A* **2013**, *117*, 6450−6457.

(40) Goulay, F.; Trevitt, A. J.; Savee, J. D.; Bouwman, J.; Osborn, D. L.; Taatjes, C. A.; Wilson, K. R.; Leone, S. R. Product Detection of the CH Radical Reaction with Acetaldehyde. *J. Phys. Chem. A* **2012**, *116*, 6091−6106.

(41) Goulay, F.; Derakhshan, A.; Maher, E.; Trevitt, A. J.; Savee, J. D.; Scheer, A. M.; Osborn, D. L.; Taatjes, C. A. Formation of Dimethylketene and Methacrolein by Reaction of the CH Radical with Acetone. *Phys. Chem. Chem. Phys.* **2013**, *15*, 4049−4058.

(42) Soorkia, S.; Taatjes, C. A.; Osborn, D. L.; Selby, T. M.; Trevitt, A. J.; Wilson, K. R.; Leone, S. R. Direct Detection of Pyridine Formation by the Reaction of CH (CD) with Pyrrole: A Ring Expansion Reaction. *Phys. Chem. Chem. Phys.* **2010**, *12*, 8750−8758.

(43) Hammond, B. L.; Lester, W. A., Jr.; Reynolds, P. J. *Monte Carlo Methods in Ab Initio Quantum Chemistry, Vol. 1 of World Scientific Lecture and Course Notes in Chemistry*; World Scientific: Singapore, 1994.

(44) Anderson, J. B. In *Reviews in Computational Chemistry*; Lipkowitz, K. B., Boyd, D. B., Eds.; John Wiley and Sons: New York, 1999; Vol. *13*, pp 133−182.

(45) Ceperley, D. M.; Mitas, L. In *New Methods in Computational Quantum Mechanics*; Prigogine, I., Rice, S. A., Eds.; John Wiley and Sons: New York, 1996; Vol. *93*, pp 1−38.

(46) Foulkes, W. M. C.; Mitas, L.; Needs, R. J.; Rajagopal, G. Quantum Monte Carlo Simulations of Solids. *Rev. Mod. Phys.* **2001**, *73*, 33−83.

(47) Helgaker, T.; Jorgensen, P.; Jeppe, O. *Molecular Electronic-Structure Theory*; John Wiley and Sons: Chichester, UK, 2000.

(48) Szabo, A.; Ostlund, N. *Modern Quantum Chemistry: Introduction to Advanced Electronic Structure Theory*; McGraw-Hill: New York, 1989.

(49) Zhao, Y.; Truhlar, D. G. The M06 Suite of Density Functionals for Main Group Thermochemistry, Thermochemical Kinetics, Non-covalent Interactions, Excited States, and Transition Elements: Two New Functionals and Systematic Testing of Four M06-class Functionals and 12 Other Functionals. *Theor. Chem. Acc.* **2008**, *120*, 215−241.

(50) Head-Gordon, M.; Pople, J. A.; Frisch, M. J. MP2 Energy Evaluation by direct methods. *Chem. Phys. Lett.* **1988**, *153*, 503−506.

(51) Krishnan, R.; Binkley, J. S.; Seeger, R.; Pople, J. A. Self-consistent Molecular Orbital Methods. XX. A Basis Set for Correlated Wave Functions. *J. Chem. Phys.* **1980**, *72*, 650−654.

(52) Gonzales, C.; Schlegel, H. B. An Improved Algorithm for Reaction Path Following. *J. Chem. Phys.* **1989**, *90*, 2154−2161.

(53) Gonzales, C.; Schlegel, H. B. Reaction Path Following in Mass-weighted Internal Coordinates. *J. Phys. Chem.* **1990**, *94*, 5523−5527.

(54) Jensen, F. *Introduction to Computational Chemistry*; John Wiley and Sons: New York, 1999; p 189.

(55) Baker, J.; Scheiner, A.; Andzelm, J. Spin Contamination in Density Functional Theory. *Chem. Phys. Lett.* **1993**, *216*, 380−388.

(56) Montoya, A.; Truong, T. N.; Sarofim, A. F. Spin Contamination in Hartree-Fock and Density Functional Theory Wavefunctions in Modeling of Adsorption on Graphite. *J. Phys. Chem. A* **2000**, *104*, 6108−6110.

(57) Wittbrodt, J. M.; Schlegel, H. B. Some Reasons not to Use Spin Projected Density Functional Theory. *J. Chem. Phys.* **1996**, *105*, 6574−6577.

(58) Cioslowski, J.; Liu, G.; Martinov, M.; Piskorz, P.; Moncrieff, D. Energetics and Site Specificity of the Homolytic C−H Bond Cleavage in Benzenoid Hydrocarbons: An ab Initio Electronic Structure Study. *J. Am. Chem. Soc.* **1996**, *118*, 5261−5264.

(59) Murray, C. W.; Handy, N. C.; Amos, R. D. A study of O_3, S_3, CH_2, and Be_2 using Kohn−Sham theory with accurate quadrature and large basis sets. *J. Chem. Phys.* **1993**, *98*, 7145−7151.

(60) Pople, J. A.; Gill, P. M. W.; Handy, N. C. Spin-Unrestricted Character of Khon-Sham Orbitals for Open-Shell Systems. *Int. J. Quantum Chem.* **1995**, *56*, 303−305.

(61) Gordon, M. S.; Schmidt, M. W. *Theory and Applications of Computational Chemistry: The First Forty Years*; Elsevier: Amsterdam, 2005.

(62) Schmidt, M. W.; Baldridge, K. K.; Boatz, J. A.; Elbert, S. T.; Gordon, M. S.; Jensen, J. H.; Koseki-Matsunaga, S. N.; Nguyen, K. A.; Su, S. J.; Windus, T. L.; Dupuis, M.; Montgomery, J. A. General Atomic and Molecular Electronic Structure System. *J. Comput. Chem.* **1993**, *14*, 1347−1363.

(63) Aspuru-Guzik, A.; Salomon-Ferrer, R.; Austin, B.; Perusquia-Flores, R.; Griffin, M. A.; Oliva, R. A.; Skinner, D.; Domin, D.; Lester, W. A., Jr. Software News and Updates Zori 1.0: A Parallel Quantum Monte Carlo Electronic Structure Package. *J. Comput. Chem.* **2005**, *26*, 856−862.

(64) Schmidt, K. E.; Moskowitz, J. W. Correlated Monte Carlo Wave Functions for the Atoms He Through Ne. *J. Chem. Phys.* **1990**, *93*, 4172−4178.

(65) Boys, S. F.; Handy, N. C. The Determination of Energies and Wavefunctions with Full Electronic Correlation. *Proc. R. Soc. London, Ser. A* **1969**, *310*, 43−61.

(66) Reynolds, P. J.; Ceperley, D. M.; Alder, B. J.; Lester, W. A., Jr. Fixed-node Quantum Monte Carlo for Molecules. *J. Chem. Phys.* **1982**, *77*, 5593−5603.

(67) Toulouse, J.; Umrigar, C. J. Optimization of Quantum Monte Carlo Wave Functions by Energy Minimization. *J. Chem. Phys.* **2007**, *126*, 084102−1−084102−16.

(68) Nicolaides, A.; Rauk, A.; Glukhovtsev, M. N.; Radom, L. Heats of Formation from G2, G2(MP2), and G2(MP2,SVP) Total Energies. *J. Phys. Chem.* **1996**, *100*, 17460−17464.

(69) Chase, M. W., Jr.; Davies, C. A.; Downey, J. R., Jr.; Frurip, D. J.; McDonald, R. A.; Syverud, A. N. JANAF Thermochemical Tables, 3rd ed. *J. Phys. Chem. Ref. Data* **1985**, *14*, Suppl. No. 1.

(70) Lias, S. G.; Bartmess, J. E.; Liebman, J. F.; Holmes, J. L.; Levin, R. D.; Mallard, W. G. Gas-phase Ion and Neutral Thermochemistry. *J. Phys. Chem. Ref. Data* **1988**, *17*, Suppl. No. 1.

(71) Kollias, A. C.; Couronne, O.; Lester, W. A., Jr. Quantum Monte Carlo Study of the Reaction: $Cl + CH_3OH \rightarrow CH_2OH + HCl$. *J. Chem. Phys.* **2004**, *121*, 1357−1363.

(72) Barker, J. R. Multiple-Well, Multiple-Path Unimolecular Reaction Systems. I. MultiWell Computer Program Suite. *Int. J. Chem. Kinet.* **2001**, *33*, 232−245.

(73) Barker, J. R. Energy Transfer in Master Equation Simulations: A New Approach. *Int. J. Chem. Kinet.* **2009**, *41*, 748−763.

(74) Barker, J. R.; Ortiz, N. F.; Preses, J. M.; Lohr, L. L.; Maranzana, A.; Stimac, P. J.; Nguyen, T. L.; Kumar, T. J. D. *MultiWell Software (v. 2014.1)*; University of Michigan: Ann Arbor, MI, 2013.

(75) Gillespie, D. T. Exact Stochastic Simulation of Coupled Chemical Reactions. *J. Phys. Chem.* **1977**, *81*, 2340.

(76) Gillespie, D. T. *Markov Processes: An Introduction for Physical Scientists*; Academic Press: San Diego, CA, 1992.

(77) Huber, K.; Herzberg, G. *Molecular Spectra and Molecular Structure 4. Constants of Diatomic Molecules*; van Nostrand: Princeton, 1979.

(78) Pople, J. A.; Head-Gordon, M.; Fox, D. J.; Raghavachari, K.; Curtiss, L. A. Gaussian-1 Theory: A General Procedure for Prediction of Molecular Energies. *J. Chem. Phys.* **1989**, *90*, 5622−5629.

(79) Curtiss, L. A.; Jones, C.; Trucks, W.; Raghavachari, K.; Pople, J. A. Gaussian-1 Theory of Molecular Energies for Second-row Compounds. *J. Chem. Phys.* **1990**, *93*, 2537−2545.

(80) Grossman, J. Benchmark Quantum Monte Carlo Calculations. *J. Chem. Phys.* **2002**, *117*, 1434−1440.

(81) Feller, D.; Peterson, K. A. Re-examination of Atomization Energies for the Gaussian-2 Set of Molecules. *J. Chem. Phys.* **1999**, *110*, 8384−8396.

(82) Pedley, J. B. *Thermodynamic Data and Structures of Organic Compounds*; Thermodynamics Research Center: College Station, TX, 1994; Vol. *1*.

(83) Ruscic, B.; Boggs, J. E.; Burcat, A.; Csaszar, A. G.; Demasison, J.; Janoschek, R.; Martin, J. M. L.; Morton, M. L.; Rossi, M. J.; Stanton, J. F.; Sazalay, P. G.; Westmoreland, P. R.; Zabel, F.; Berces, T. IUPAC Critical Evaluation of Thermochemical Properties of Selected Radicals. Part I. *J. Phys. Chem. Ref. Data* **2005**, *34*, 573−656.

(84) Asatryan, R.; Silva, G.; da Bozzelli, J. W. Quantum Chemical Study of the Acrolein (CH_2CHCHO) + OH + O_2 Reactions. *J. Phys. Chem. A* **2010**, *114*, 8302−8311.

(85) Li, Y.; Baer, T. The Dissociation Dynamics and Thermochemistry of the Acrolein Ion Studied by Threshold Photoelectron−photoion Coincidence Spectroscopy. *Int. J. Mass Spectrom.* **2002**, *218*, 37−48.

(86) Rodriquez, C. F.; Bohme, D. K.; Hopkinson, A. C. Theoretical Enthalpies of Formation of CH_mCl_n: Neutral Molecules and Cations. *J. Phys. Chem.* **1996**, *100*, 2942−2949.

(87) Feller, D.; Franz, J. A. A Theoretical Determination of the Heats of Formation of Furan, Tetrahydrofuran, THF-2-yl, and THF-3-yl. *J. Phys. Chem. A* **2000**, *104*, 9017−9025.

(88) Curtiss, L. A.; Raghavachari, K.; Redfern, P. C.; Pople, J. A. Assessment of Gaussian-2 and Density Functional Theories for the Computation of Enthalpies of Formation. *J. Chem. Phys.* **1997**, *106*, 1063−1079.